

## Research Article

# Dynamical Analysis of an Interleaved Single Inductor TITO Switching Regulator

**Abdelali El Aroudi,<sup>1</sup> Vanessa Moreno-Font,<sup>2</sup> and Luis Benadero<sup>2</sup>**

<sup>1</sup> *Departament d'Enginyeria Electrònica, Elèctrica i Automàtica (DEEEA), Universitat Rovira i Virgili, Tarragona, Spain*

<sup>2</sup> *Departament de Física Aplicada, Universitat Politècnica de Catalunya, Barcelona, Spain*

Correspondence should be addressed to Abdelali El Aroudi, [abdelali.elaroudi@urv.cat](mailto:abdelali.elaroudi@urv.cat)

Received 1 December 2008; Revised 24 February 2009; Accepted 7 April 2009

Recommended by José Roberto Castilho Piqueira

We study the dynamical behavior of a single inductor two inputs two outputs (SITITO) power electronics DC-DC converter under a current mode control in a PWM interleaved scheme. This system is able to regulate two, generally one positive and one negative, voltages (outputs). The regulation of the outputs is carried out by the modulation of two time intervals within a switching cycle. The value of the regulated voltages is related to both duty cycles (inputs). The stability of the whole nonlinear system is therefore studied without any decoupling. Under certain operating conditions, the dynamical behavior of the system can be modeled by a piecewise linear (PWL) map, which is used to investigate the stability in the parameter space and to detect possible subharmonic oscillations and chaotic behavior. These results are confirmed by numerical one dimensional and two-dimensional bifurcation diagrams and some experimental measurements from a laboratory prototype.

Copyright © 2009 Abdelali El Aroudi et al. This is an open access article distributed under the Creative Commons Attribution License, which permits unrestricted use, distribution, and reproduction in any medium, provided the original work is properly cited.

## 1. Introduction

Switching power converters are widely used in the power management area, due to their high efficiency, low cost and small size [1]. In most of the applications, these systems are used in situations where there is a need to stabilize an output voltage to a desired constant value. However, there are other applications where more than one output must be controlled. For instance, the portable equipments in modern vehicles such mobile phones, MP3 players, PDAs, GPS usually include a variety of loads such as LCD displays, memories, microprocessors, Universal Series Bus (USB) and Hard Disk Drives (HDD). These loads require different operating voltages and load currents and are powered by the rechargeable batteries through DC-DC converters. To make the system run life be longer and its size smaller, more and more system designers are focusing on improving the system power conversion efficiency with advanced power converters topologies. The traditional solution of

using independent converters, one for each output, has the shortcomings of higher number of switches and magnetics components. Besides this option and other dual DC-DC converter configurations [2–6], single inductor multiple input multiple output (SIMIMO) DC-DC converters are, in general, convenient solutions for these low power applications.

Recently, a great variety of complex nonlinear behaviors are studied in simple power electronic circuits like DC-DC converters [7–19]. These studies, which are based on obtaining accurate mathematical models, have allowed a deep understanding of their fundamental properties and dynamic behavior. Obtaining these mathematical models is a traditional challenge for the power electronics engineers and there exist in the recent literature many efforts devoted to this research area (see [2–14] and references therein). The main drawback of the models obtained is their complexity which prevents the obtaining of clear system design criteria in terms of the parameters. Pioneer references about these topics can be found in the works reported in [8, 9], where the first studies about the existence of bifurcations and chaotic behavior in buck converters controlled by PWM are done. We can also mention other related works in this research field in the recent literature [10–13] for the buck converter under voltage mode control and [14–16] for different types of power electronic converters.

Nowadays, there are many works dealing with nonlinear behavior in elementary stand alone [19] and other more complex power electronics circuits such as paralleled DC-DC converters [20], multicell and multilevel converters [21–23] and also for an example of single inductor two inputs two outputs (SITITOs) converters [17].

In this paper, more insights into the modeling and analysis of an SITITO interleaved converter are presented. After presenting the switched model, a systematic approach is described to obtain a simple PWL map that can be used to predict accurately the fast scale (switching) dynamics of the system. The model will be used to get some analytical conditions for stability of the system and for optimizing its performance.

The rest of the paper is organized as follows. Section 2 deals with the description of the SITITO DC-DC converter and the basis for the interleaving control circuit is presented. Then in Section 3, the general mathematical model is given. Under the assumption of perfect output regulation, the general PWL map is derived. Section 4 will deal with stability analysis by using this PWL map. We will use the derived map to get some analytical expressions for stability conditions and to draw some bifurcation curves of the system. In Section 5 we deal with numerical simulations from the PWL map and we obtain some one-dimensional and two-dimensional bifurcation diagrams of the system by using this map. Experimental validation of our analytical and simulation results is presented in Section 6. Finally, some conclusions are given in the last section.

## **2. Single Inductor TITO DC-DC Regulator**

### **2.1. Power Stage Circuit**

The schematic diagram in Figure 1 shows a DC-DC converter with a single inductor for two outputs  $v_P$  and  $v_N$  with opposite polarity. Both loads, considered here as equivalent resistances  $R_N$  and  $R_P$ , can be powered from the power source  $V_{in}$  by generating a sequence of command signals driving switches  $S_A$  and  $S_B$ .

### **2.2. Pulse Width Modulation Strategy with Interleaving**

The control strategy for the SITITO topology of Figure 1, which is used in this paper and was proposed in [18], is shown in Figure 2.

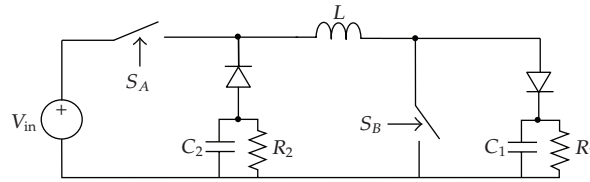


**Figure 1:** Schematic diagram of a single inductor DC-DC converter with positive  $v_P$  and negative  $v_N$  output voltages.

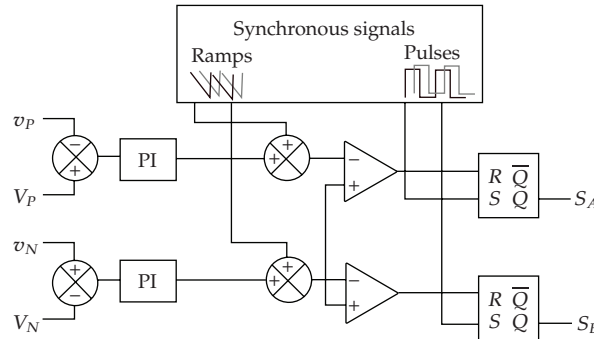


**Figure 2:** Control strategy of single inductor two outputs converter of Figure 1 based on interleaved pulse width modulation.

This interleaved current mode control works as follows: from the set of input-output errors, two dynamical references, which are associated to each of the channels, are obtained. Each of these reference signals is added to an appropriate phase-shifted (interleaved) compensating ramp  $v_r^j$ , so that in the steady state regime, a sequence of time intervals, once per channel, will be produced. In this way, the ramp signal  $v_r^j$ ,  $j \in \{A, B\}$ ) corresponding to channel  $j$  is shifted by a phase shift  $\phi_j$ . Based on current mode control, the general idea is to obtain a current reference  $I_r^j$  for each channel (output) and to use two comparators. The particular reference  $I_r^j$  is formed by a single compensating ramp and a combination of the output of the PI error filtering blocks. This signal is to be compared to the inductor current  $i_L$ . It is demonstrated in [17] that in order to achieve stable behavior, each of the channels should use just the output of the PI corrector coming from the other one. That is switch  $S_A$ , which controls the time interval during which current is delivered to the negative output, must be driven accordingly to the error produced by the positive output. Likewise, switch  $S_B$ , which affects the positive output, is driven by the error of the negative output. The regulation is possible because of the crossed effect produced when considering the whole system (power stage plus control).

### 3. Closed Loop Mathematical Modeling

#### 3.1. Switched Model for the SITITO Converter

The switched model of the system can be summarized in the set of five equations (3.1)–(3.5), each of them providing the evolution of the corresponding state variable [17]. The various configurations of the system are taken into account through the binary control signals  $u_A$

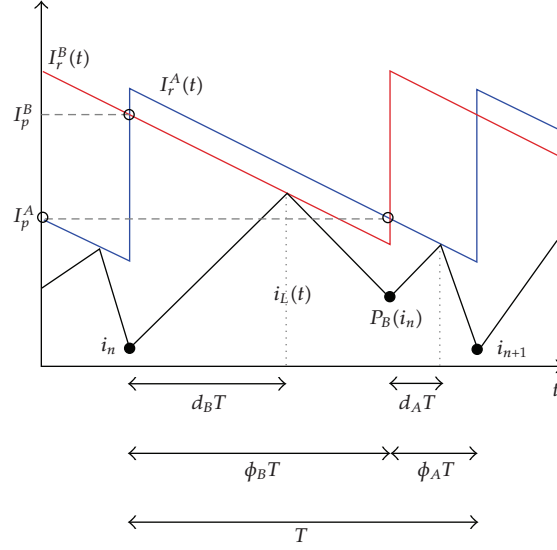


Figure 3: Control signals for the SITITO interleaved DC-DC converter.

and  $u_B$  imposed by the state of the switches. This model can be easily obtained by applying standard Kirchhoff's voltage law to the circuit. In doing so, we obtain:

$$\frac{dv_P}{dt} = \frac{1}{C_P} \left( i_L(1 - u_B) - \frac{v_P}{R_P} \right), \quad (3.1)$$

$$\frac{dv_N}{dt} = \frac{1}{C_N} \left( -i_L(1 - u_A) - \frac{v_N}{R_N} \right), \quad (3.2)$$

$$\frac{ds_P}{dt} = \frac{1}{\tau_P} (V_P - v_P), \quad (3.3)$$

$$\frac{ds_N}{dt} = \frac{1}{\tau_N} (v_N - V_N), \quad (3.4)$$

$$\frac{di_L}{dt} = \frac{1}{L} ((u_B - 1)v_P + (1 - u_A)v_N - r_L i_L + V_{in} u_A), \quad (3.5)$$

where  $v_P$  is the voltage across the capacitor  $C_P$ ,  $v_N$  is the voltage across the capacitor  $C_N$ ,  $i_L$  is the current through the inductor  $L$  whose equivalent series resistance is  $r_L$ .  $R_P$  and  $R_N$  are the resistive loads for both outputs.  $s_P$  and  $s_N$  are the integral variables, being  $\tau_P$ ,  $\tau_N$ ,  $V_P$  and  $V_N$  the respective time constants and voltage references.  $u_A$  and  $u_B$  are the driving binary signal which are 1 if the corresponding switch is "on" and 0 if the switch is "off". To help with comprehension of the action of the control, relevant control signals and parameters are shown in Figure 3. In this figure,  $I_r^A$  and  $I_r^B$  are the reference currents that can be expressed as:

$$I_r^A(t) = \frac{1}{r_S} \left( g_P (V_P - v_P + s_P) + v_r^A(t) \right), \quad (3.6)$$

$$I_r^B(t) = \frac{1}{r_S} \left( g_N (v_N - V_N + s_N) + v_r^B(t) \right),$$

being  $v_r^A(t)$  and  $v_r^B(t)$  are the ramp signals defined as following:

$$\begin{aligned} v_r^A(t) &= V_u - (V_u - V_l) \bmod \left( \frac{t}{T}, 1 \right), \\ v_r^B(t) &= V_u - (V_u - V_l) \bmod \left( \frac{t}{T} - \phi_B, 1 \right), \end{aligned} \quad (3.7)$$

where  $\bmod(\cdot)$  stands for the modulo function and  $\phi_A = 1 - \phi_B$ .

The first subset of (3.1) and (3.2) refers to the dynamics of the voltage outputs  $v_P$  and  $v_N$ . Additional subset (3.3) and (3.4) deals with two equations for each of the integral terms  $s_P$  and  $s_N$  and (3.5) refers to the inductor current dynamics. During each switching period the switch  $S_A$  (resp.,  $S_B$ ) is closed for a time duration  $d_A T$  (resp.,  $d_B T$ ). The duty ratio for each “on” sub-interval ( $d_A$  or  $d_B$ ), which is determined by the action of its comparator, can be expressed implicitly in terms of the state variables as follows:

$$\begin{aligned} I_r^A(t) - i_L &= 0, \\ I_r^B(t) - i_L &= 0. \end{aligned} \quad (3.8)$$

Obtaining  $d_A$  and  $d_B$  requires solving (3.8). It should be noted that these conditions should apply to the equations of  $I_r^A(t)$  and  $I_r^B(t)$  in the configuration before the asynchronous switching instant, and if they are not feasible and  $i_L(T) < I_r^j(\phi_j T)$  then  $d_j$  is set to  $\phi_j$  whereas it is set to 0 if  $i_L(T) > I_r^j(\phi_j T)$ . By combining (3.1)–(3.5) with (3.8), we obtain the closed loop switched continuous time model that can be used for computer simulations. Figure 4 depicts the waveforms of the state variables of the system of the above described model from numerical simulation. Note that the output voltages are well regulated to their respective references ( $V_P = 3$  V and  $V_N = -15$  V) and also that the integral variables are almost constant.

### 3.2. Piecewise Linear Map

In this section we will try to give a one dimensional map that can capture the fast-scale dynamic assuming that the slow dynamics due to the external feedback loops are stable. The complete discrete modeling of the dynamics of a SITITO converter can be described by a five dimensional nonlinear piecewise smooth map. Under the assumption that all outputs are well regulated to their desired references, this map can be simplified by a one-dimensional map in which only the discrete time inductor current  $i_n := i_L(nT)$  remains a state variable. This assumption is valid if the period of the modulating signal  $T$  is much lower than the time constants or periods (in case of oscillators) of every operating topology and the PI controller is designed to provide a stable slow dynamics. In this situation, the ripples of all capacitor voltages are small and consequently, these variables can be approximated by their averaged values, which are forced by the PI controller to be equal to the reference voltages (Figure 4). The state variables  $s_P$  and  $s_N$  can also be considered constant whose values can be well obtained by using the averaged model [17]. Due to the different operating modes that the system can present ( $d_A$  and  $d_B$  nonsaturated and saturated), the one-dimensional map has

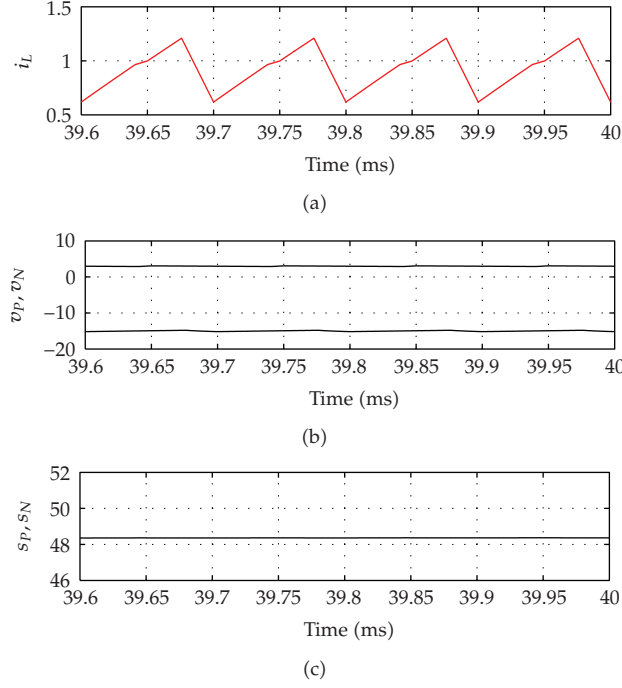


**Figure 4:** Waveforms of the state variables of the interleaved SITITO converter.  $V_{in} = 6$  V,  $V_P = 3$  V,  $V_N = -15$  V,  $V_u = 1$  A. Other parameter values are those of Table 1.

different forms. Independently of the operating mode, it can be shown that the map can be written in the following form:

$$i_{n+1} = P(i_n) = P_A \circ P_B(i_n), \quad (3.9)$$

where  $P_j$  is the local sub-mapping defined by:

$$P_j(x) = \begin{cases} x + m_{\text{on}}\phi_j T, & \text{if } d_j > \phi_j, \\ x + m_{\text{on}}d_j T + m_{\text{off}}^j(\phi_j - d_j)T, & \text{if } d_j < \phi_j, \end{cases} \quad (3.10)$$

where  $j \in \{A, B\}$  in the subscript case and  $j \in \{P, N\}$  in the superscript case,  $x$  is the state variable at the beginning of phase  $j$ , and  $m_{\text{on}}$  and  $m_{\text{off}}^j$  are the approximated slopes of the inductor current during the “on” and the “off” configuration of both phases, which are given by:

$$\begin{aligned} m_{\text{on}} &= \frac{V_{\text{in}} - r_L I_L}{L}, \\ m_{\text{off}}^P &= \frac{V_{\text{in}} - V_P - r_L I_L}{L}, \\ m_{\text{off}}^N &= \frac{V_N - r_L I_L}{L}. \end{aligned} \quad (3.11)$$

This model applies if  $P_j(x) > 0$ . In the case that  $P_j(x) < 0$ ,  $P(x)$  is set to zero and the converter is said to work in the discontinuous conduction mode (DCM). This last mode is taken into account in all numerical simulation. In the expressions of  $m_{\text{on}}$ ,  $m_{\text{off}}^P$  and  $m_{\text{off}}^N$  the term  $r_L i_L$ , which appears in the inductor current state equation, was approximated by  $r_L I_L$ , where the parameter  $I_L$  is obtained by means of the averaged model and it is given by [17]:

$$I_L = \frac{V_{\text{in}}}{2r_L} + \sqrt{\frac{V_{\text{in}}^2}{4r_L^2} - \frac{1}{r_L} \left( \frac{V_P^2}{R_P} + \frac{V_N(V_N - V_{\text{in}})}{R_N} \right)}. \quad (3.12)$$

The duty cycles  $d_A$  and  $d_B$  are obtained by assuming that the inductor current is linear during each charging phase. Using this assumption gives the following expressions:

$$d_A = \frac{I_p^A - i_n^A}{(m_{\text{on}} - m_r)T'}, \quad (3.13)$$

$$d_B = \frac{I_p^B - i_n^B}{(m_{\text{on}} - m_r)T'}$$

where  $i_n^B = i_n$  and  $i_n^A = P_B(i_n)$ .  $I_p^A$  and  $I_p^B$  are respectively the value of  $I_r^A(t)$  and  $I_r^B(t)$  at the beginning of phases  $A$  and  $B$  and

$$m_r = -\frac{V_u - V_l}{r_S T} \quad (3.14)$$

is the slope of the ramp signals  $v_r^A$  and  $v_r^B$ . To obtain  $I_p^A$  and  $I_p^B$ , we consider that the inductor current is PWL and that the duty cycles corresponding to both phases are given from the averaged model by:

$$D_A = \phi_A - \left| \frac{V_N}{R_N I_L} \right|, \quad (3.15)$$

$$D_B = \phi_B - \left| \frac{V_P}{R_P I_L} \right|.$$

The values of  $I_p^A$  and  $I_p^B$ , which do not depend on  $i_n$  are, therefore, obtained using the following area condition:

$$\int_0^T i_L(t) dt = I_L T. \quad (3.16)$$

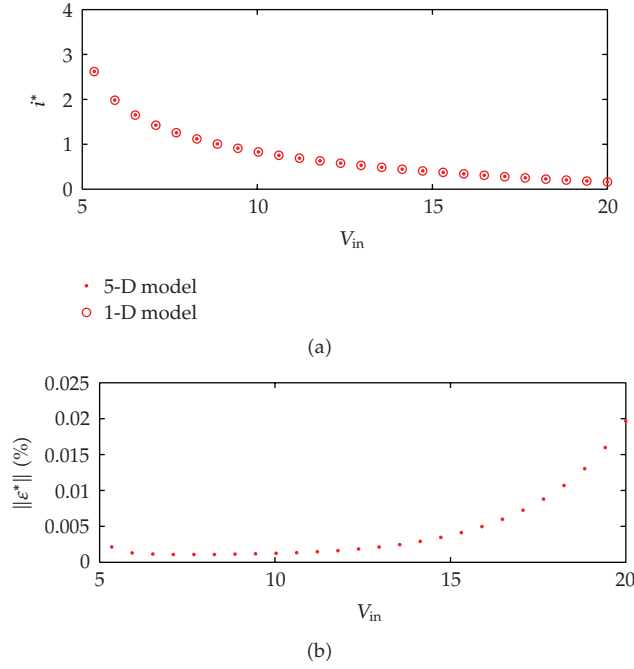


**Figure 5:** The fixed point  $i^*$  obtained from the 1D approximated model and the 5D exact model.

The fixed point  $i^*$  is obtained by forcing that  $i_{n+1} = i_n = i^*$ . This gives the following expression for  $i^*$ :

$$\begin{aligned}
 i^* = I_L + & \left( \left( \frac{(D_A^2 + D_B^2)}{2} - \phi_A D_A - 2\phi_B D_B \right) m_{on} \right. \\
 & + \left( 2\phi_B D_B - \frac{3\phi_B^2}{2} + \frac{D_B^2}{2} \right) m_{off}^A \\
 & \left. + \left( \phi_A D_A - \frac{D_A^2}{2} - \frac{\phi_B^2}{2} \right) m_{off}^A \right) T.
 \end{aligned} \tag{3.17}$$

This expression is then used to calculate  $I_p^A$  and  $I_p^B$ . The one-dimensional map has a single nonsaturated fixed point  $i^*$  which corresponds to the one periodic orbit of the switching system. Figure 5 gives the evolution of  $i^*$  when the input voltage varies. The result is obtained both numerically by using the exact 5D discrete time model and analytically by using (3.17). As it can be observed, the results match very well and the maximum error  $\|\epsilon\|_{\max}$  is less than 0.6%.

Figure 6 shows the cobweb plot of the map  $P$  for different values of  $V_p$ . Note the richness of behaviors that the map can exhibit. Namely, in Figure 6(a) we can see the coexistence of two different attractors of the system. The system will evolve toward an attractor or toward another depending on the starting point (initial condition). In Figure 6(b), dead beat phenomenon is observed. In this case, the system makes one and only one cycle

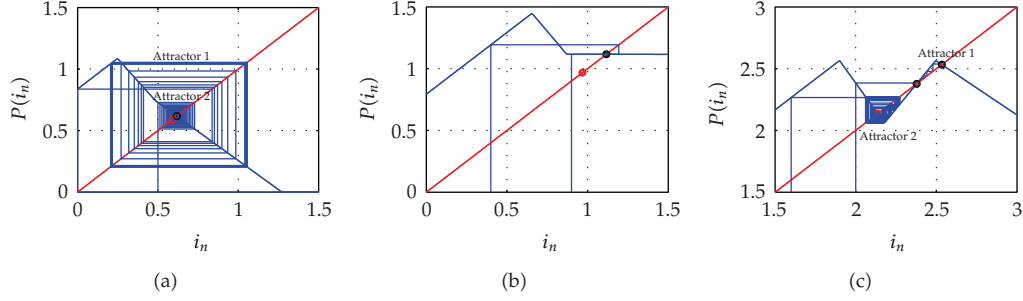


**Figure 6:** Cobweb plot of the map  $P$  for different values of  $V_p$ . (a)  $V_p = 3$  V, (b)  $V_p = 8.27$  V, (c)  $V_p = 14$  V.  $V_u = 0.5$  A.

to arrive to the fixed point once the trajectory hits the horizontal line defining the PWL map. Figure 6(c) presents the behavior of the system after a pitchfork bifurcation and its associated coexistence of attractors.

## 4. Stability Analysis from the PWL Map

### 4.1. The Stability Index

A sufficient condition for stability is that the absolute value of the derivative  $\lambda$  of the map  $P$  evaluated at the fixed point  $i^*$  is smaller than 1. It can be shown that this derivative is:

$$\lambda = \frac{(m_{\text{off}}^P - m_r)(m_{\text{off}}^N - m_r)}{(m_{\text{on}} - m_r)^2}, \quad (4.1)$$

and in terms of parameters of the system,  $\lambda$  becomes:

$$\lambda = \frac{(V_{\text{in}} - V_p - r_L I_L + (L(V_u - V_i)/T))(V_N - r_L I_L + (L(V_u - V_i)/r_S T))}{(V_{\text{in}} - r_L I_L + (L(V_u - V_i)/r_S T))^2}. \quad (4.2)$$

It can be observed that  $\lambda$  is a function of all parameters of the system. Let us define the following set of parameters:

$$\begin{aligned} \kappa &= \frac{L(V_u - V_i)}{r_S T}, \\ \alpha &= r_L I_L - V_{\text{in}} + V_p, \\ \beta &= r_L I_L + V_N, \\ \gamma &= r_L I_L - V_{\text{in}}. \end{aligned} \quad (4.3)$$

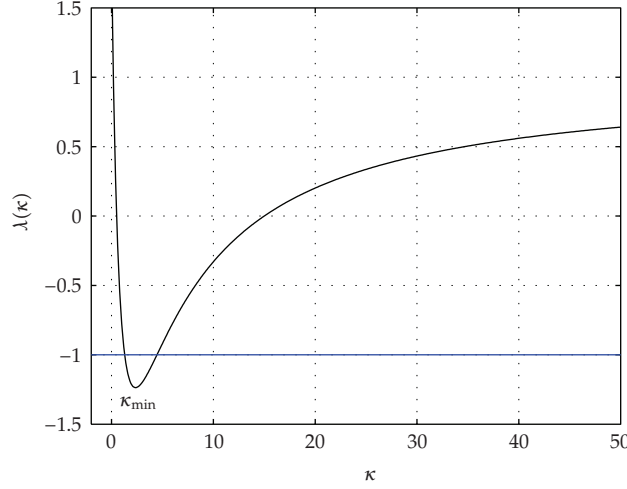


**Figure 7:** The stability index as function of  $\kappa$ .  $\alpha = 0.5$ ,  $\beta = 5$  and  $\gamma = -2$ .

Note that in the above expressions  $\kappa > 0$  and  $V_{in} > 0$ . With these definitions the stability index  $\lambda$  becomes

$$\lambda(\kappa) = \frac{(\kappa - \alpha)(\kappa - \beta)}{(\kappa - \gamma)^2}. \quad (4.4)$$

This index should be between  $-1$  and  $1$  in order to get a stable behavior. If this is not fulfilled, the system may present many nonlinear phenomena in the form of bifurcations, subharmonic oscillations and chaotic behavior. Considering the term  $r_L I_L \ll V_{in}$  which is the case in practical circuits, and taking into account that under this assumption, the parameters fulfill conditions:  $\beta > 0$ ,  $\gamma < 0$ , and  $\alpha > \gamma$ , the function  $\lambda(\kappa)$  has the following properties (see Figure 7).

- (i) The asymptotic value of  $\lambda$  is  $\lim_{\kappa \rightarrow \infty} \lambda(\kappa) = 1$ .
- (ii) Although the index  $\lambda(\kappa)$  has a singular point at  $\kappa = \gamma$ , this is not reachable provided that  $\kappa$  must be positive.
- (iii) The index  $\lambda(\kappa)$  has a minimum value at  $\kappa_{min}$  ( $(d\lambda/d\kappa)(\kappa_{min}) = 0$ )

$$\kappa_{min} = \frac{-\beta\gamma + \alpha\gamma - 2\alpha\beta}{-\alpha - \beta + 2\gamma}. \quad (4.5)$$

#### 4.2. Nonsmooth Flip Bifurcation ( $\lambda(\kappa) = -1$ ) Curves

Flip bifurcation can appear for a nonlinear system if for a certain set of parameter values one have  $\lambda(\kappa) = -1$ . For our system, this will be possible if

$$\kappa_{min} = \frac{-\beta\gamma + \alpha\gamma - 2\alpha\beta}{-\alpha - \beta + 2\gamma} < -1. \quad (4.6)$$

Then, the critical values of  $\kappa$  where the bifurcation flip can appear are given by the expression:

$$\kappa_{\text{flip}} = \frac{1}{4} \left( \alpha + \beta + 2\gamma \pm \sqrt{(\alpha - \beta)^2 - 4(\alpha - \gamma)(\beta - \gamma)} \right). \quad (4.7)$$

Notice that this bifurcation will be given only if  $\kappa_{\text{flip}}$  is a real positive number, that is,

$$(\alpha - \beta)^2 - 4(\alpha - \gamma)(\beta - \gamma) > 0 \quad \text{or} \quad \alpha + \beta + 2\gamma > \sqrt{(\alpha - \beta)^2 - 4(\alpha - \gamma)(\beta - \gamma)}. \quad (4.8)$$

### 4.3. Nonsmooth Pitchfork ( $\lambda(\kappa) = 1$ ) Bifurcation Curves

If for a certain choice of parameter values one have  $\lambda(\kappa) = 1$ , then a nonsmooth pitchfork bifurcation occurs. The critical value of  $\kappa$  for which this bifurcation takes place is given by the expression:

$$\kappa_p = \frac{\alpha\beta - \gamma^2}{\alpha + \beta - 2\gamma}. \quad (4.9)$$

This bifurcation will actually appear if  $\kappa$  is positive, that is,

$$\alpha\beta > \gamma^2 \quad (4.10)$$

which will be never reached if  $\alpha < 0$ . Therefore, this bifurcation cannot appear if  $V_{\text{in}} > V_P$  (see Figures 6(a) and 6(b)) and it is possible if  $V_{\text{in}} < V_P$  (see Figure 6(c)).

### 4.4. Dead-Beat Response ( $\lambda(\kappa) = 0$ ) Curves

A dead beat response to a small disturbance in the state of the system can be achieved by setting  $\lambda(\kappa_{\text{db}}) = 0$  (Figure 6(b)). This implies the following relation between the parameters:

$$\kappa_{\text{db}} = \alpha \quad \text{or} \quad \kappa_{\text{db}} = \beta, \quad (4.11)$$

which corresponds to the following choice of circuit parameters:

$$\frac{L(V_u - V_l)}{r_S T} = V_P - V_{\text{in}} + r_L I_L \quad \text{or} \quad \frac{L(V_u - V_l)}{r_S T} = r_L I_L - V_N. \quad (4.12)$$

As it can be observed, this condition depends on parasitic parameters and therefore it will be difficult to meet in practical circuit. However it will be always the optimal choice of circuit parameters to get the fastest response. Figure 8 shows the different possible bifurcation curves in the plane  $(\alpha, \kappa)$ . The dead-beat response curves ( $\lambda = 0$ ) is also shown in the same figure.

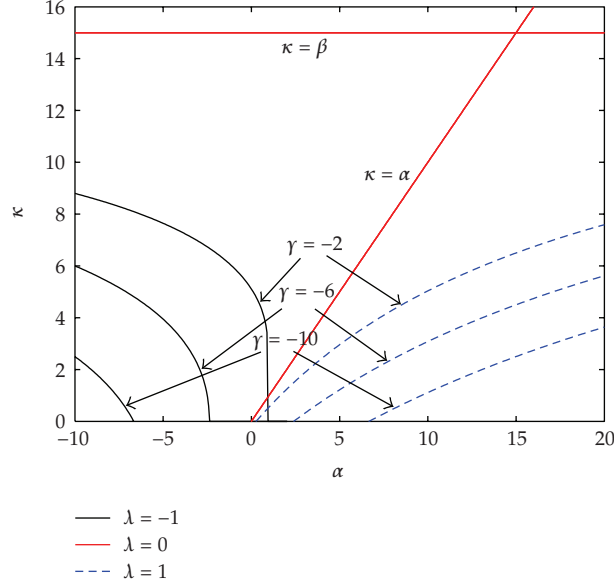


Figure 8: The bifurcation curves in the plane  $(\alpha, \kappa)$  for different values of  $\gamma$ .  $\beta = 15$ .

Table 1: Parameter values used in numerical simulations.

Parameter	Value	Parameter	Value
$V_{in}$	Varying	$V_l$	0
$L$	640 $\mu\text{H}$	$V_u$	Varying
$r_L$	0.7 $\Omega$	$V_P$	Varying
$C_N$	45 $\mu\text{F}$	$V_N$	-15 V
$C_P$	45 $\mu\text{F}$	$\tau_A$	200 $\mu\text{s}$
$R_N$	68 $\Omega$	$\tau_B$	200 $\mu\text{s}$
$R_P$	33 $\Omega$	$g_P$	0.02 $\Omega^{-1}$
$f_s = 1/T$	10 kHz	$g_N$	0.02 $\Omega^{-1}$
$r_S$	1 $\Omega$	$\phi_A = \phi_B$	1/2

## 5. Bifurcation Behavior from Numerical Simulation

After undergoing a bifurcation, the period  $\tau$  of a possible periodic orbit of the nonlinear system is an integer multiple of the period of the forcing ramp signal, that is,  $\tau = nT$ , where  $n = 1, 2, \dots$ . Such an operation of the converter will be referred to as an  $n$ -periodic orbit.

### 5.1. Bifurcations from the PWL Map

Let us consider the circuit of Figure 1 with the control scheme of Figure 2 and the values of parameters shown in Table 1. The bifurcation parameter used here is the upper value of the ramp voltage  $V_u$ . From mathematical analysis of the PWL map, the boundary of stability in terms of the parameters can be obtained. Two critical values, corresponding to flip curves, are

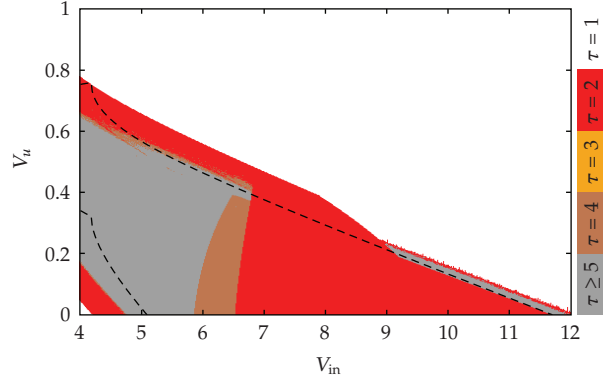


**Figure 9:** Two-dimensional bifurcation diagram taking  $V_u$  and  $V_{in}$  as bifurcation parameter. Initial conditions are selected in the vicinity of the DC averaged state  $I_L$ .  $V_P = 3$  V.

derived for the amplitude of the ramp voltage  $V_u$  in terms of other bifurcation parameters. These critical values are given by:

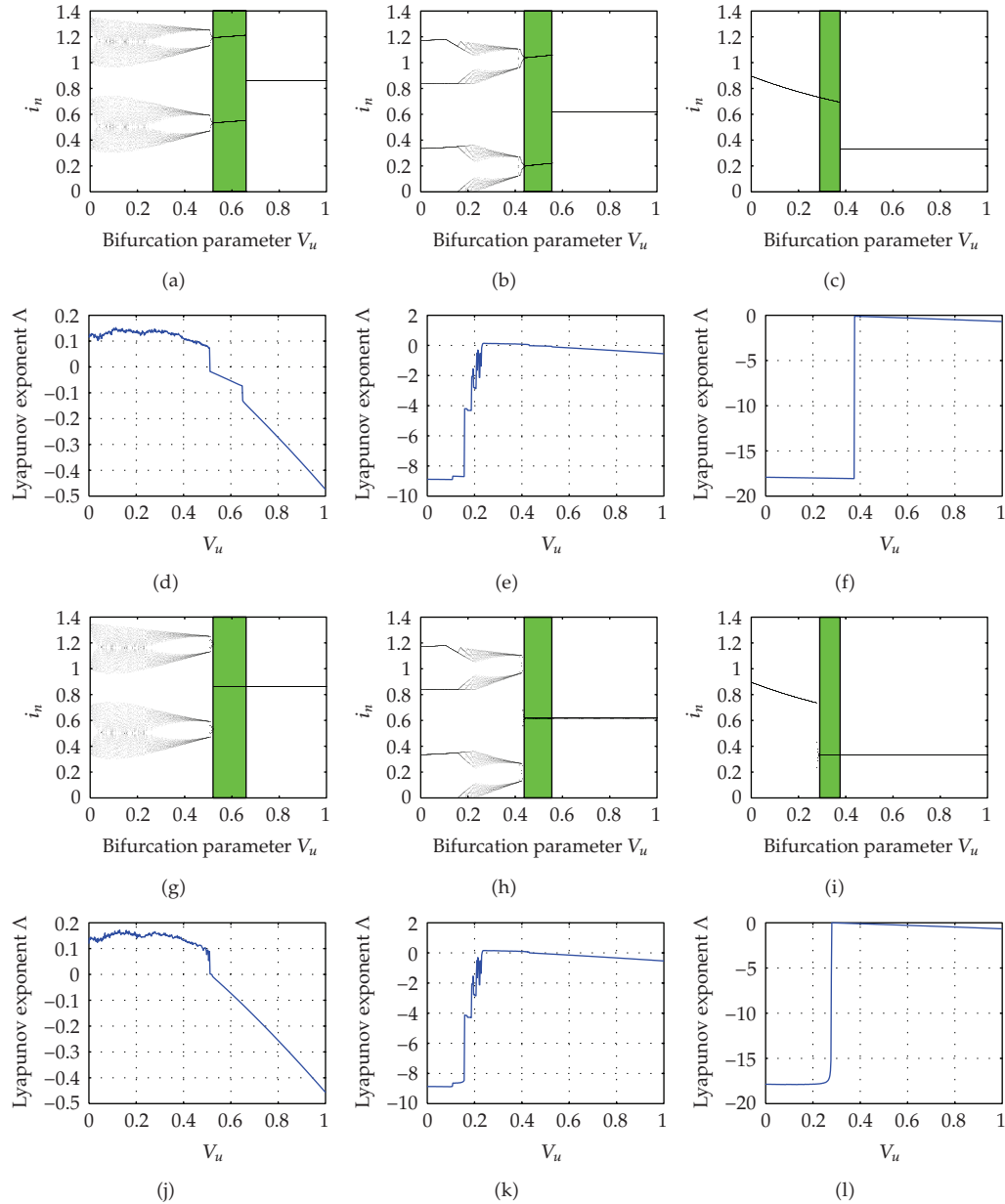
$$V_{u,cri,1} = r_L I_L + \frac{r_S T \left( V_P - 3V_{in} - V_N - \sqrt{(V_P)^2 + 6V_P(V_N - V_{in}) + (V_N - V_{in})^2} \right)}{4L}, \quad (5.1)$$

$$V_{u,cri,2} = r_L I_L + \frac{r_S T \left( V_P - 3V_{in} - V_N + \sqrt{(V_P)^2 + 6V_P(V_N - V_{in}) + (V_N - V_{in})^2} \right)}{4L}.$$

Note that theoretically there exist two different critical values of  $V_u$  for which stability is lost. However some times one of the critical values is virtual because it is complex or negative. One way to avoid instability and subharmonic oscillations is by making both critical values virtual. This can be achieved if the following condition is fulfilled:

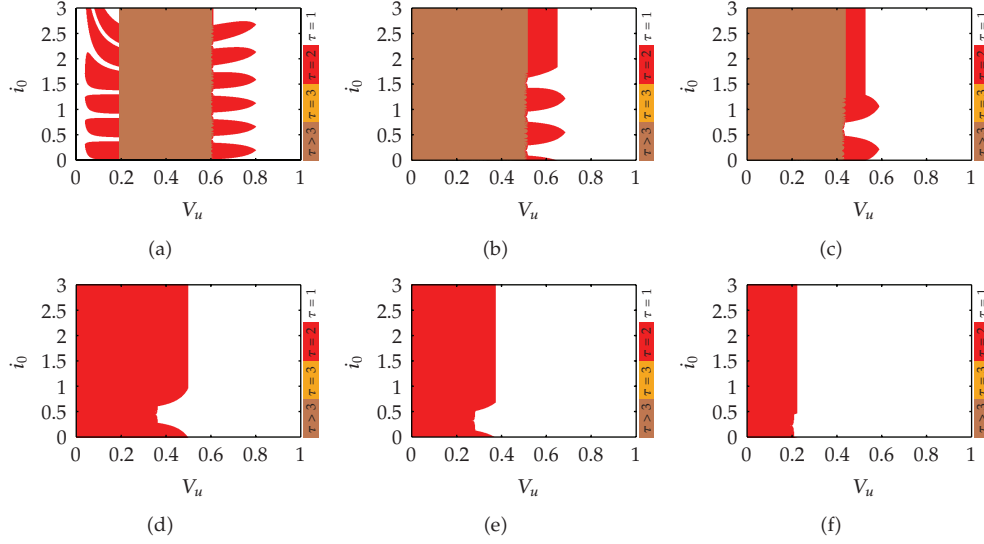
$$(V_P)^2 + 6V_P(V_N - V_{in}) + (V_N - V_{in})^2 < 0. \quad (5.2)$$

Figure 9 shows the two dimensional bifurcation diagram obtained from numerical simulations by using the PWL discrete time model derived in the previous section. The analytical expressions giving conditions for stability of 1-periodic orbits are also plotted in the same figure (black dashed lines). As it can be observed, theoretical analysis and numerical simulations are in good agreement on the stability boundary of the 1-periodic orbits. It can be shown by mathematical analysis that the 1-periodic and the 2-periodic orbits have the same stability boundary although their domains of existence are different. This means that these two orbits will coexist in a certain zone of the parameter space and depending on the initial conditions the final state could be a 1-periodic or a 2-periodic orbit. In order to put more clear this coexisting attractors phenomenon, the one-dimensional bifurcation diagrams and their corresponding Lyapunov exponents are plotted in Figure 10 for different values of the input voltage and choosing differently the initial conditions. The hysteresis phenomenon, due to the coexistence of attractors within a certain interval of the bifurcation parameter, is reflected



**Figure 10:** One dimensional bifurcation diagram and Lyapunov exponent taking  $V_u$  as bifurcation parameter for different values of  $V_{in}$ . (a)–(f) initial conditions are selected in the vicinity of  $I_L$ . (g)–(l) initial conditions are selected in the vicinity of  $i^*$ . From left to right  $V_{in} = 5, 6, 8V$ . Shaded area shows hysteresis interval whose width decreases when  $V_{in}$  increases.

as a shaded area in this figure. The width of this interval decreases when  $V_{in}$  increases. The basin of attraction of an attractor, which is defined as the set of points in the state space such that initial conditions chosen in this set dynamically evolve to this attractor, can be obtained by sweeping the initial  $i_0$  condition in a certain interval of the bifurcation parameter. The evolution of the basins of attraction of the different possible attractors in terms of  $V_u$  are



**Figure 11:** Evolution of the basins of attractions in terms of  $V_u$  for different values of  $V_{in}$  (a)  $V_{in} = 4$  V, (b)  $V_{in} = 5$  V (c)  $V_{in} = 6$  V, (d)  $V_{in} = 7$  V, (e)  $V_{in} = 8$  V and (f)  $V_{in} = 9$  V.

shown in Figure 11 for different values of  $V_{in}$ . In Figures 9 and 11, the period of the orbit was color coded. Only five colors were used to determine the different periodic modes that the system can present. Using more colors does not change the results because the system does not present stable periodic orbit with period bigger than four in this case. White color represent the stable zone (1-periodic). Zones of higher periods and chaotic behavior are also shown as parameters  $V_u$  and  $V_{in}$  vary. Particularly, we observe from Figure 9 for example that when  $V_{in} = 6$  V and as  $V_u$  decreases the inductor current is 1-periodic then at a critical value of  $V_u$  becomes 2-periodic and suddenly becomes chaotic after a border collision bifurcation at another critical value of  $V_u$ . As  $V_u$  decreases further, the inductor current becomes 4-periodic. This is in a good concordance with the one-dimensional bifurcation diagram and the evolution of the Lyapunov exponent in Figure 10. The Lyapunov exponent is a measure of average amount of contraction or expansion of a trajectory near a periodic orbit and it is defined as follows:

$$\Lambda = \lim_{N \rightarrow \infty} \frac{1}{N} \sum_{n=1}^N \ln \left| \frac{dP(i_n)}{di_n} \right|. \quad (5.3)$$

Due to the nonsmooth nature of the system, the map  $P$  is PWL and its derivative  $dP(i_n)/di_n$  is piecewise constant. Therefore the Lyapunov exponent can undergo jumps at some bifurcation points.

## 5.2. Bifurcations from the Exact Switched Model

The above results were derived from the PWL map of the SITITO converter where  $v_P$  and  $v_N$  and the integral terms  $s_P$  and  $s_N$  are assumed constant. Therefore, it is necessary to check how these results are close to the actual system behavior when this assumption is not made

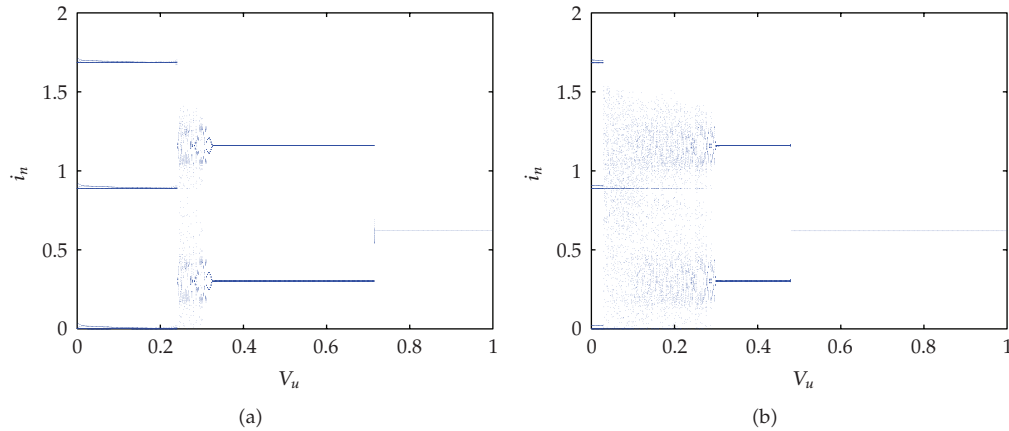


**Figure 12:** One dimensional bifurcation diagram from the 5D switched model taking  $V_u$  as bifurcation parameter for  $V_{in} = 6$  V.

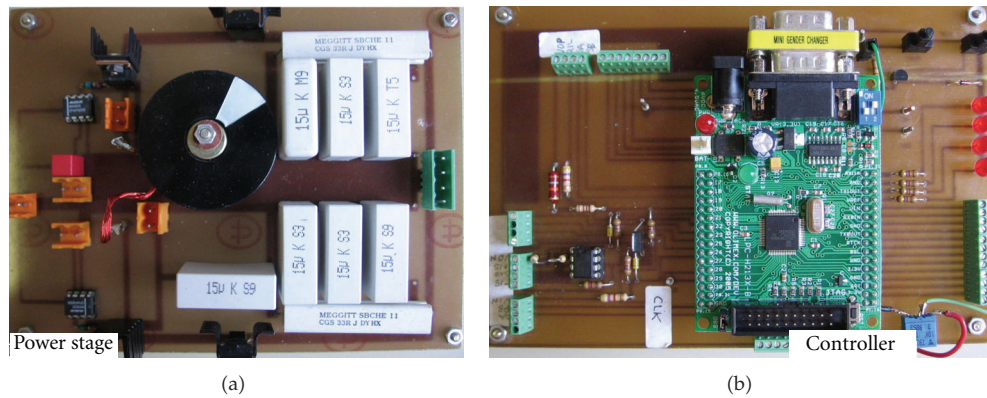


**Figure 13:** Experimental prototype of a SITTIO DC-DC converter. (a) Power stage circuit. (b) PWM Interleaved controller.

and the output voltage ripples are taken into account. Figure 12 shows two representative bifurcation diagrams of the system from simulation of the circuit diagram using the switched model, in which the parameter  $V_u$  was varied as before. The parameter  $V_{in}$  is fixed to 6 V and all other parameter values and details are the same as for the above subsection. In one case the bifurcation parameter is increased while in another case it is decreased. In this way, initial conditions are chosen differently. Comparing Figures 12(a) and 12(b) from one side with Figures 10(b) and 10(h) from the other side, the first aspect in which the actual system dynamical behavior is different from that derived from the PWL map is that in the zone of small values of  $V_u$  which is not used in practical circuits. Another difference is the parameter value for which the first period doubling occur is a little bit different. Thus there is a range of parameters where the 2-periodic is stable for the exact model while the PWL map predict 1-periodic stable. Apart from this aspect, the prediction of the simplified model regarding transition from periodicity to chaos and coexisting attractors is enough accurate in almost all the parameter range from  $V_u \approx 0.3$  V to  $V_u = 1$  V.

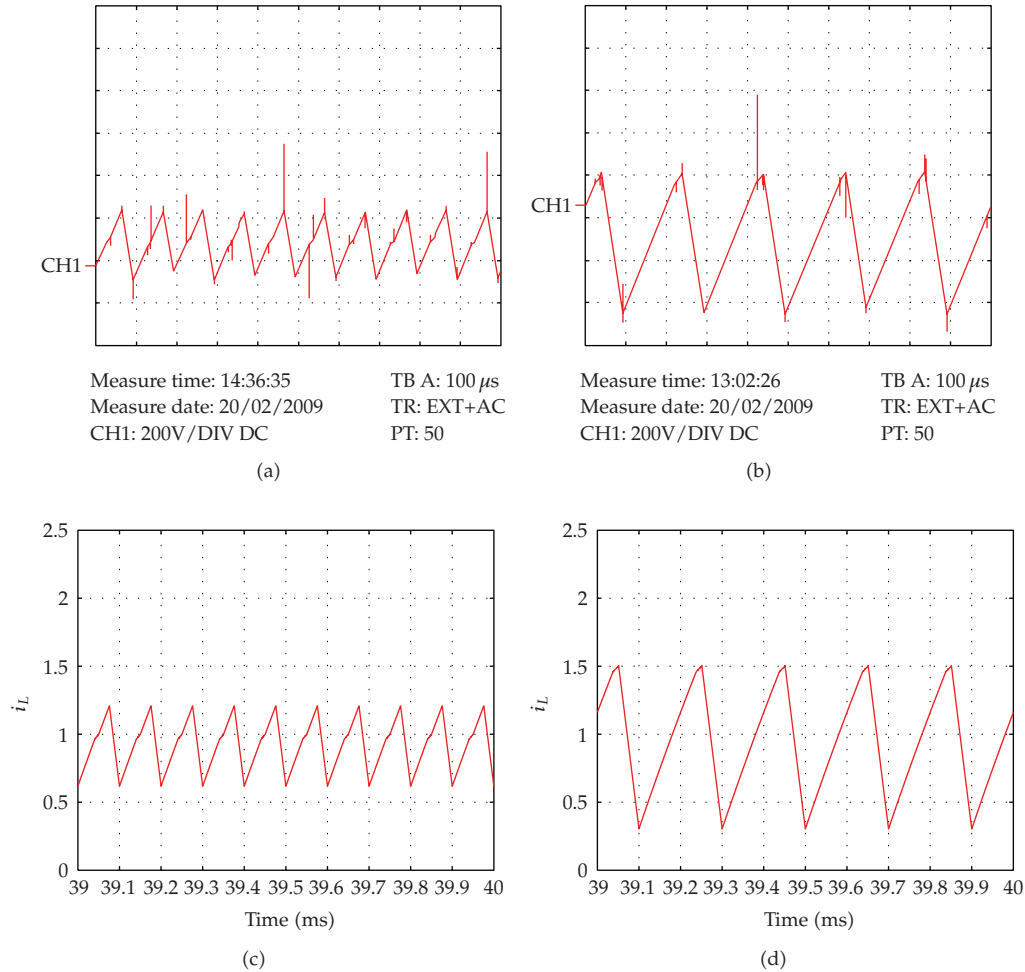


**Figure 14:** Experimental waveforms of the inductor current and their corresponding numerical simulations from the switched model showing normal periodic behavior (left  $V_u = 1\text{ V}$ ), subharmonic oscillations (2-periodic) (right  $V_u = 0.6\text{ V}$ ) after losing the stability of the 1-periodic orbit by a nonsmooth flip bifurcation. Other parameters are from Table 1.

## 6. Experimental Results

A prototype of a SITITO DC-DC converter (Figure 13) has been built in order to confirm our analytical results and numerical simulations. The nominal values of parameters are the same than previous sections. The inductor current is sensed using the LEM current probe PR30. The control signals are obtained and processed by a microcontroller. This device provides the command signals which are buffered by two dedicated MOS drivers from MAXIM (MAX626), then they are applied to the MOSFET IRF9Z34S ( $p$ -channel) and IRL530N ( $n$ -channel). Diodes in Figure 1 are Schottky barrier type (6CWQ04FN). The inductor current  $i_L$  is represented with a proportional voltage with a factor of 0.5 V/A. The phases  $\phi_A$  and  $\phi_B$  are selected slightly different from  $(1/2)$  (0.55 and 0.45) to avoid some noise effects at the switching instants. From the point of view of dynamics, the ranges for some parameters have been chosen accordingly with our technical resources, but the results can

be rescaled, for instance, under higher switching frequencies and lower inductance, unless parasitic components effects become relevant. Figure 14 shows the experimental waveforms of the inductor current for the normal periodic behavior and subharmonic oscillations. Numerical simulations from the switched model are also shown for comparison. As it can be observed, except some noise at the switching instants, there is a good agreement between the experimental and the numerical results.

## 7. Conclusions

A single inductor two inputs two outputs (SITITO) DC-DC converter under current mode control with an interleaved PWM control strategy is considered in this paper. Its dynamics is described by a nonlinear modeling approach. The ripple, mainly the associated to the inductor current, and saturation effects can cause instabilities in the form of subharmonic oscillations and chaotic behavior. An expression for a simple PWL map is derived to obtain accurate information about the dynamics of the system. This map can predict many nonlinear behaviors such as bifurcations, chaos, coexisting attractors and the associated hysteresis phenomenon. Numerical simulations and experimental measurements from a laboratory prototype confirm the theoretical predictions.

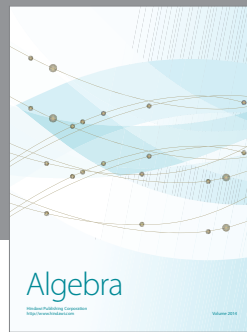
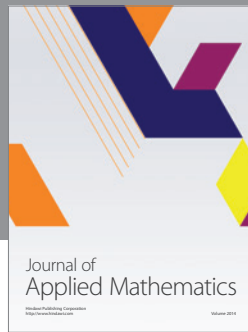
## Acknowledgments

The authors would like to thank the anonymous reviewers for their valuable comments and suggestions. This work was partially supported by the Spanish MSI under Grants TEC-2007-67988-C02-01 and ENE2005-06934/ALT.

## References

- [1] R. W. Erickson and D. Maksimovic, *Fundamentals of Power Electronics*, Springer, New York, NY, USA, 2001.
- [2] I. Dénes and I. Nagy, "Two models for the dynamic behaviour of a dual-channel buck and boost DC-DC converter," *Electromotion*, vol. 10, no. 4, pp. 556–561, 2003.
- [3] H.-P. Le, C.-S. Chae, K.-C. Lee, G.-H. Cho, S.-W. Wang, and G.-H. Cho, "A single-inductor switching DC-DC converter with 5 outputs and ordered power-distributive control," *IEEE Journal of Solid-State Circuits*, vol. 42, no. 12, pp. 2706–2714, 2007.
- [4] J. Hamar and I. Nagy, "Asymmetrical operation of dual channel resonant DC-DC converters," *IEEE Transactions on Power Electronics*, vol. 18, no. 1, part 1, pp. 83–94, 2003.
- [5] R. Barabás, B. Buti, J. Hamar, and I. Nagy, "Control characteristics, simulation and test results of a dual channel DC-DC converter family," in *Proceedings of Power Electronics Electrical Drives Automation and Motion Conference (SPEEDAM '04)*, Capri, Italy, June 2004.
- [6] Y. Xi and P. K. Jain, "A forward converter topology with independent and precisely regulated multiple outputs," *IEEE Transactions on Power Electronics*, vol. 18, no. 2, pp. 648–658, 2003.
- [7] S. Banerjee and G. C. Verghese, *Nonlinear Phenomena in Power Electronics: Bifurcations, Chaos, Control, and Applications*, Wiley-IEEE Press, New York, NY, USA, 2001.
- [8] D. C. Hamill and D. J. Jeffries, "Subharmonics and chaos in a controlled switched-mode power converter," *IEEE Transactions on Circuits and Systems*, vol. 35, no. 8, pp. 1059–1061, 1988.
- [9] J. H. B. Deane and D. C. Hamill, "Instability, subharmonics, and chaos in power electronic systems," *IEEE Transactions on Power Electronics*, vol. 5, no. 3, pp. 260–268, 1990.
- [10] E. Fossas and G. Olivar, "Study of chaos in the buck converter," *IEEE Transactions on Circuits and Systems I*, vol. 43, no. 1, pp. 13–25, 1996.
- [11] S. Banerjee, M. S. Karthik, G. Yuan, and J. A. Yorke, "Bifurcations in one-dimensional piecewise smooth maps—theory and applications in switching circuits," *IEEE Transactions on Circuits and Systems I*, vol. 47, no. 3, pp. 389–394, 2000.

- [12] Z. T. Zhusubaliyev and E. Mosekilde, *Bifurcations and Chaos in Piecewise-Smooth Dynamical Systems*, vol. 44 of *World Scientific Series on Nonlinear Science. Series A*, World Scientific, River Edge, NJ, USA, 2003.
- [13] S. Banerjee and K. Chakrabarty, "Nonlinear modeling and bifurcations in the boost converter," *IEEE Transactions on Power Electronics*, vol. 13, no. 2, pp. 252–260, 1998.
- [14] M. di Bernardo and C. K. Tse, "Chaos in power electronics: an overview," in *Chaos in Circuits and Systems*, G. Chen and T. Ueta, Eds., vol. 11, chapter 16, pp. 317–340, World Scientific, New York, NY, USA, 2002.
- [15] C. K. Tse and M. Di Bernardo, "Complex behavior in switching power converters," *Proceedings of the IEEE*, vol. 90, no. 5, pp. 768–781, 2002.
- [16] L. Benadero, A. El Aroudi, G. Olivar, E. Toribio, and E. Gómez, "Two-dimensional bifurcation diagrams. Background pattern of fundamental DC-DC converters with PWM control," *International Journal of Bifurcation and Chaos in Applied Sciences and Engineering*, vol. 13, no. 2, pp. 427–451, 2003.
- [17] L. Benadero, R. Giral, A. El Aroudi, and J. Calvente, "Stability analysis of a single inductor dual switching DC-DC converter," *Mathematics and Computers in Simulation*, vol. 71, no. 4–6, pp. 256–269, 2006.
- [18] L. Benadero, V. Moreno-Font, A. El Aroudi, and R. Giral, "Single inductor multiple outputs interleaved converters operating in CCM," in *Proceedings of the 13th International Power Electronics and Motion Control Conference (EPE-PEMC '08)*, pp. 2115–2119, Poznan, Poland, September 2008.
- [19] A. El Aroudi, M. Debbat, R. Giral, G. Olivar, L. Benadero, and E. Toribio, "Bifurcations in DC-DC switching converters: review of methods and applications," *International Journal of Bifurcation and Chaos in Applied Sciences and Engineering*, vol. 15, no. 5, pp. 1549–1578, 2005.
- [20] H. H. C. Iu and C. K. Tse, "Bifurcation behavior in parallel-connected buck converters," *IEEE Transactions on Circuits and Systems I*, vol. 48, no. 2, pp. 233–240, 2001.
- [21] A. El Aroudi, M. Debbat, and L. Martínez-Salamero, "Poincaré maps modeling and local orbital stability analysis of discontinuous piecewise affine periodically driven systems," *Nonlinear Dynamics*, vol. 50, no. 3, pp. 431–445, 2007.
- [22] B. Robert and A. El Aroudi, "Discrete time model of a multi-cell DC/DC converter: non linear approach," *Mathematics and Computers in Simulation*, vol. 71, no. 4–6, pp. 310–319, 2006.
- [23] A. El Aroudi, B. G. M. Robert, A. Cid-Pastor, and L. Martínez-Salamero, "Modelling and design rules of a two-cell buck converter under a digital PWM controller," *IEEE Transactions on Power Electronics*, vol. 23, no. 2, pp. 859–870, 2008.



# Hindawi

Submit your manuscripts at  
<http://www.hindawi.com>

